A PVT Cooling System Design and Realization: Temperature Effect on the PV Module Performance Under Real Operating Conditions

Charaf Hajjaj*, Mohammadi Benhmida*‡, Rachid Bendaoud*, Houssam Amiry*, Said Bounouar*, Abdellatif Ghennioui**, Fatima Chanaa*, Said Yadir*,***, Ahmed Elhassnaoui*,****, Hassan Ezzaki*,

* Laboratory of Electronics, Instrumentation and Energetic, Faculty of Sciences, Chouaïb Doukkali University, B.P 20, El Jadida, Morocco

** Research Institute for Solar Energy and New Energies (IRESEN), Green Energy Park, Benguerir, Morocco

*** Laboratory of Materials, Processes, Environment and Quality, ENSA, Cadi Ayyad University, Safi, Morocco

**** Industrial Engineering Laboratory, Faculty of Science and Technology, BP: 523, Beni Mellal, Morocco

(hajjaj.c@ucd.ac.ma, benhmida.m@ucd.ac.ma, rbendaoud27@gmail.com, houssam.amiry@gmail.com, bounouar.said@gmail.com, ghennioui@iresen.org, fatimachanaa2020@gmail.com, yadir1976@yahoo.fr, ahmed.elhassnaoui@gmail.com, ahmed.elhassnaoui@gmail.com)

‡Corresponding Author; Mohammadi Benhmida, Route Ben Maachou B.P 20, 24000, El Jadida, Morocco, Tel: +212 6 82 08 04 75, Fax: +212 523 342 187, benhmida.m@ucd.ac.ma

Received: 12.11.2018 Accepted:12.01.2019

Abstract- It is established that the efficiency of the most common solar cells decreases when their temperature increases. The photovoltaic module characteristics, especially its efficiency and its maximum power, are defined in standard test conditions (STC), while their nominal operating temperature is higher than ambient temperature and depending on operating conditions of the photovoltaic module. Thus, it is important to characterize the photovoltaic module performance under real operating conditions and for different temperature values. This study involves the design and realization of a cooling system of a monocrystalline photovoltaic module by a sheet of water circulating on its backside, while keeping its temperature values 2 to 3 degrees higher than the cooling water temperature. This system is investigated numerically to determine the configuration enabling a good control of the temperature on photovoltaic module surface. The realized and described hybrid system in this paper was intended to validate results of the optimal configuration obtained by simulation based on finite element method. The extraction and comparison of physical parameters of the cooled photovoltaic module with those of a similar reference module without cooling system are described.

Keywords Heat transfer, Hybrid Photovoltaic-Thermal collector (PVT), Photovoltaic cell efficiency.

1. Introduction

The efficiency of photovoltaic modules available on the market is more or less dependent on their operating temperature [1]. Several studies of hybrid Photovoltaic-Thermal (PVT) system [2–17] were developed to control the photovoltaic module temperature and recover the thermal energy dissipated as a form of heat as well as to characterize the temperature effect on different photovoltaic (PV) modules. Tripanagnostopoulos et al [18] carried out a comparative study on several hybrid systems (PVT, PVT+ booster diffuse reflector, PVT + glazing + booster diffuse reflector) using water or air as a coolant. The results of this study show that the electrical efficiency of the PVT/water system is 13.3% higher than the PV module, which has back surface thermally insulated. Furthermore, it is 3.2% higher than the PV module with a natural convection in front and back sides. Chow et al. [19] studied several PVT collectors. They found that glazed PVT collectors have better thermal efficiencies than unglazed ones. While unglazed collectors

deal better with electrical efficiency. Yang et al [20] designed a PVT system by integrating photovoltaic cells on a substrate through a functionally graded material with water tubes cast inside to improve their electrical and thermal efficiency. Rossi et al [21] investigated numerically and experimentally several configurations of a cooling system with circulating water in a serpentine circuit. The results of their study show that the temperature differences on the PV module surface can reach 10 °C. It results in a restriction of the delivered electrical power due to cells operating at highest temperatures as well as constraints able to cause a faster degradation of the semiconductor material. This PVT system provides a temperature control of the PV module in the range of 30 to 40 °C and a combined thermal and electrical efficiency of 71%. In their review [22] on hybrid PVT systems, Michael et al. (2015) compared the electrical and thermal efficiencies of different PVT technologies using several coolants. They found that thermal and electrical efficiencies superior to 80% and 20% respectively, could be obtained using diffuse reflectors and water as a coolant. Increase of more than 50% in thermal efficiency can be achieved by directly bonding PV cells to the heat absorber, with simultaneous improvement in electrical efficiency due to improved heat transfer.

Liang et al. [23] performed a hybrid PVT collector consisting of PVT module and an absorber tube crossing a specific layer filled with graphite. A thermal insulator was packed underneath the absorber collector to limit heat escaping and to ensure more uniform temperatures throughout the system. Electrical efficiency and primary energy efficiency of PVT collector was found respectively to be 7.2% and 45%.

Indoor experiments made with PVT systems using water and MWCNT water nanofluid were performed for different flow rates for a fixed solar irradiance, and ambient temperature [24]. The objective was to validate a three-dimensional numerical analysis of PVT systems with a software based on finite element method (FEM). Improvements in thermal efficiency founded numerically and experimentally were in good agreement.

It has been observed in the literature that most PVT systems using water as a coolant are based on serpentine or channel configuration for cooling the PV module. Therefore, this kind of configurations produces high temperature gradient on the PV module surface.

In this paper a new design of a PVT system with a sheet of flowing water as a cooling device with several inputs/outputs (I/O) of the coolant is presented. Numerical simulations have been performed to determine the number of coolant I/O required to maintain the temperature differences between six points chosen on the surface of the PV module less than 3 degrees. The simulations are based on exchange equations between the PVT layers, whose three-dimensional numerical resolution is performed by the software using FEM method. Evaluation of the temperature effect on physical parameters of the PV module is provided considering two solar cell models: the so-called efficient model [25] and the simple single-diode model, using Ortiz-Condé method's [26].

Nomenclature:

PV	Photovoltaic
PVT	Photovoltaic-Thermal hybrid solar collector
STC	Standard Test Conditions [Ta = 25 °C and G_n = 1000 W/m²]
EVA	Ethylene-Vinyl Acetate
FEM	Finite Element Method
MSE	Model with a single diode
q_{lw}	Radiation heat losses [W m^{-2}]
ε	Material emissivity
σ	Stefan-Boltzmann constant [W m^{-2} K^{-4}]
T_{PV}	PV module temperature [°C]
T_n	Nominal temperature of the PV module [°C]
T_a	Ambient temperature [°C]
G	Irradiation intensity [W/m²]
G_n	Irradiation intensity at STC [W/m²]
h_{wind}	Heat transfer coefficient by convection [W m^{-2} K^{-1}]
V_{wind}	Wind speed [m/s]
u	Fluid velocity [m/s]
R_S	Series resistance [Ω]
R_{SH}	Shunt resistance [Ω]
R_{PV}	Fictitious resistance [Ω]
I	Output current [A]
I_{ph}	Photocurrent generated by the module [A]
I_{SC}	Short circuit current [A]
I_0	Saturation current intensity [A]
I_m	Maximum current intensity [A]
$I_{SC,n}$	Short circuit current at STC [A]
$I_{ph,n}$	Photogenerated current intensity at STC [A]
V_{OC}	Open circuit voltage [V]
V_m	Voltage at the maximum power point [V]
V	Output voltage [V]
$V_{OC,n}$	Open circuit voltage at STC [V]
$V_{t,n}$	Module thermal voltage at STC [V]
n	Ideality factor
V_t	Module thermal voltage [V]
N_S	Cells number connected in series
q	Electron charge [=1.602×10^{-19} C]
k_B	Boltzmann constant [=1.3806×10^{-23} J/K]
K_I	Current temperature coefficient [A/°C]
N_p	Solar cells associated in parallel
M	Slope of I-V curve

E_g Band gab energy [eV]

T_{NOCT} Nominal operating cell temperature [°C]

2. Materials and methods

2.1. Experimental setup

2.1.1. PVT cooling system

Two monocrystalline photovoltaic modules (Model TDC-M20-36) were fixed on a support allowing their inclination by an angle ranging from 0 to 90 ° with the horizontal (Fig. 1.). One of the modules served as a reference, while the second was equipped with a cooling system using water as a coolant which included the following elements:

- a number of input-output (I/O) openings designed in such way that is possible to have 4, 8 or 12 balanced I/O,
- a set of vinyl pipes allowing regular distribution at the same rate on all cooling system supply tubes,
- a water reservoir supplying the system with the coolant under a constant level kept by overflow,
- a variable flow rate pump placed at the bottom of the water tank.

Initially, the PVT system was filled with water and left under solar radiation intensity until it reached a stable temperature. When temperature reached 48 °C, the coolant flow rate process was launched in order to decrease and control the PV module temperature. Simultaneously, the electrical characteristics for four temperature values were taken.

Fig. 1. PVT system. (1) Solarimeter-SL 200; (2) Control and data acquisition board; (3) Thermal camera; (4) Thermocouple; (5) Adjustable flow rate water pumping system; (6) Data recording (Computer).

Table 1. Photovoltaic modules characteristics provided by the manufacturer in STC

Technical parameter	
Model	TDC-M20-36
Cell type	Monocrystalline 62.5 * 25mm (5 inches)
Maximum power (P_{max}) [W]	20
Maximum current intensity (I_{max}) [A]	1.07
Voltage at the maximum power point (V_{max}) [V]	18.76
Short circuit current (I_{SC}) [A]	1.22
Open circuit voltage (V_{OC}) [V]	21.24
Size (mm)	534x294x20
Glass façade	2.8 mm, high transmission, low iron content, tempered glass.
Cells number connected in series (N_S)	36
Temperature correction coefficients for P_{max} (%)	-0.435
Temperature correction coefficients for I_{SC} (%)	0.043
Temperature correction coefficients for V_{OC} (%)	-0.35

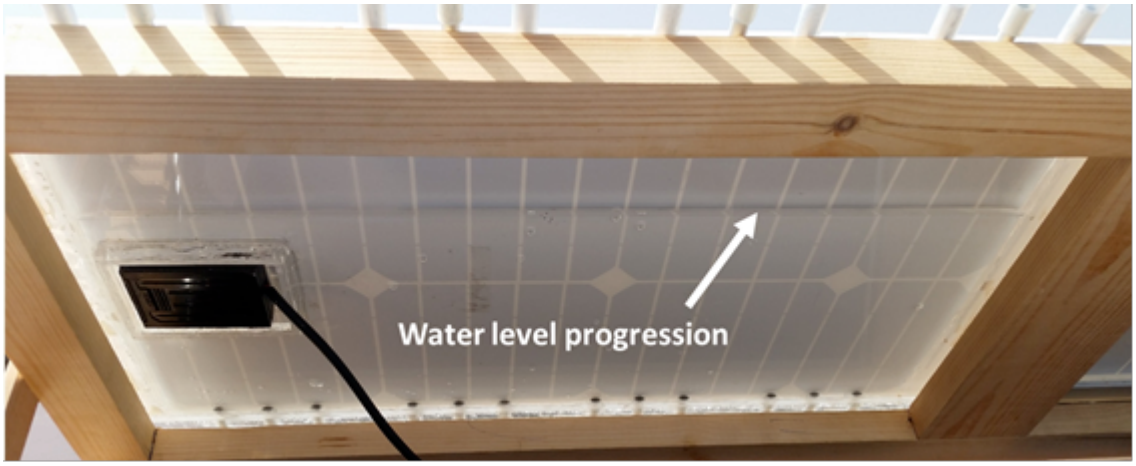

Fig. 2. Water level progression along the water sheet surface.

2.1.2. Data recording

Fig. 3 shows the experimental setup. Solar irradiance was measured on the PV module plane with SL200-Solarimeter. An implemented electronic circuit [27] was used in order to make the load resistance vary and to measure the output voltage, the terminal current, and the operating temperature using current, voltage, and temperature sensors adapted to Arduino board. The electronic circuit and sensors were controlled by the Arduino board. Thermal images were recorded by an infrared camera as described below. All collected data were stored in a computer memory.

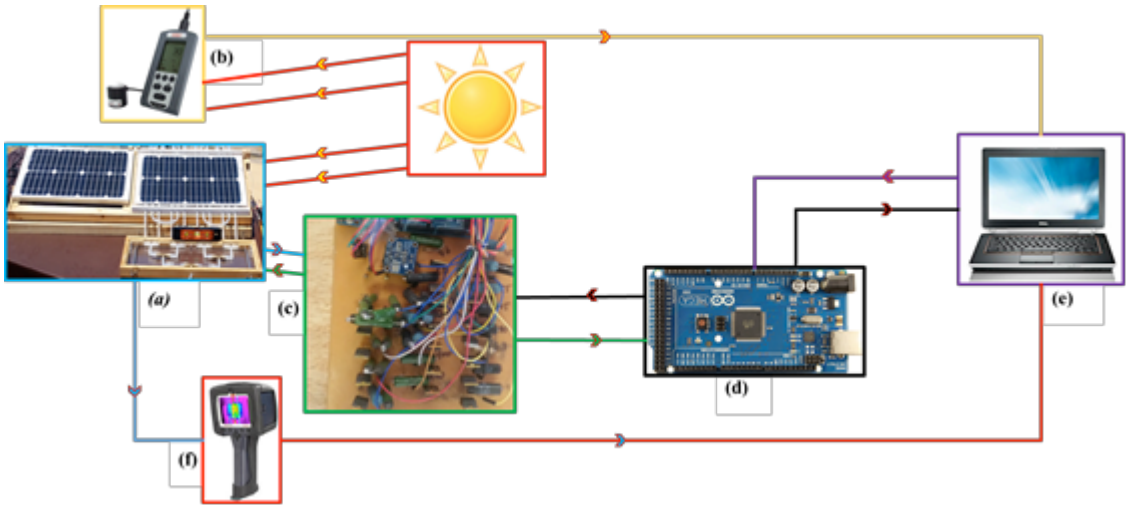

Fig. 3. Experimental setup. (a) PVT system, (b) solarimeter-SL200, (c) electronic circuit with sensors, (d) Arduino board, (e) computer.

2.1.3. Measurements of solar irradiance and PV module temperature

A thermal infrared (Flir E40) camera was used to record the thermal images of the two PV modules. The configuration of the thermal infrared camera takes into consideration ambient temperature, relative humidity and distance between the camera and the target object. The technical specifications of this thermal camera are shown in Table 2.

The global irradiance[28,29] was measured using Solarimeter-SL200 fixed to the PV modules support. The solarimeter is equipped with a data storage memory and recorded values are averaged over one minute.

2.1.4. Electrical characteristic

Current-voltage characteristics of the cooled and reference PV modules were recorded using the Arduino board [26, 27]. A program stored on its memory allows to control the load resistance change (RC).

The step of RC change in the neighboring region of was about 0.4 Ω. Each point of the current-voltage characteristic (I-V) was measured in about one millisecond. Experimental characteristics involving 132 points were plotted under constant solar irradiance. Current-voltage characteristics at operating temperatures of 24°, 33°, 37° and 48°C were measured for irradiance and wind speeds of 830 W/m², and 3.7 m/s, respectively.

Table 2. Technical specifications of the used infrared thermal camera (FLIR E40).

Parameters	Range
Temperature Range	-4°F to 1202°F (-20°C to 650°C)
Field of view/min focus distance	25° x 19° / 1.31ft (0.4m)
Resolution	19,200 (160x120) pixel
Thermal sensitivity	<0.07°C at 30°C
Frame rate	60 HZ
Detector Type (FPA)	160 x 120 pixels
Spectral range	7.5 to 13µm
Measurement correction	Reflected ambient temperature & emissivity correction

2.2. Modeling

2.2.1. Cooling system simulation

The cooling system configurations (Fig. 4) were simulated using finite element method (FEM). Three configurations (Fig. 4) were selected to show the founded optimal configuration of the cooling system. The configurations are distinguished by the number and the distribution of inputs/outputs openings: 4 (I/O), 6 (I/O) and 8 (I/O). Thickness and thermal conductivity of each layer of the PVT system were considered (Table 3).

	Thickness (mm)	Thermal Conductivity (W/m.K)
PV Glass	2.8	1.8
EVA	0.5	0.35
PV Cell	0.3	148
Tedlar	0.1	0.2
Heat exchanger	10	0.184

Energy exchanges by conduction, convection and radiation were evaluated. Several flow rates of the coolant were tested (Eq.3 and Eq.4). Stefan-Boltzmann law [31,32] allows to determine heat losses by radiation (Eq.1) towards external environment:

$$q_{lw} = \varepsilon\sigma\left(T^4 - T_a^4\right) \quad (1)$$

Where ε , σ , T and are material emissivity, Stefan-Boltzmann constant, PV module temperature and ambient temperature, respectively.

Heat transfer coefficient by convection (h_{wind}) was estimated using the method proposed by MacAdams [33]:

$$h_{wind} = 5.7 + 3.8 \times V_{wind} \quad (2)$$

Where V_{wind} is the wind speed.

The fluid was supposed incompressible with a laminar flow. The equation of continuity (Eq.3) and Navier-Stockes equation (Eq.4) [34] were considered:

$$\nabla(\rho u) = 0 \quad (3)$$

$$\nabla(\rho u) = -\nabla P + \mu\nabla^2 u + \rho g \quad (4)$$

Where u, ρ, P and μ are speed (m/s), density (kg/m3), pressure (Pa) and viscosity (Pa.s) of the coolant. g is the gravitational acceleration (m/s²), respectively.

Six representative points (T1, T2 ..., T6) (Fig. 4) on the cooled module surface were selected to evaluate the evolution of their temperatures according to the operating

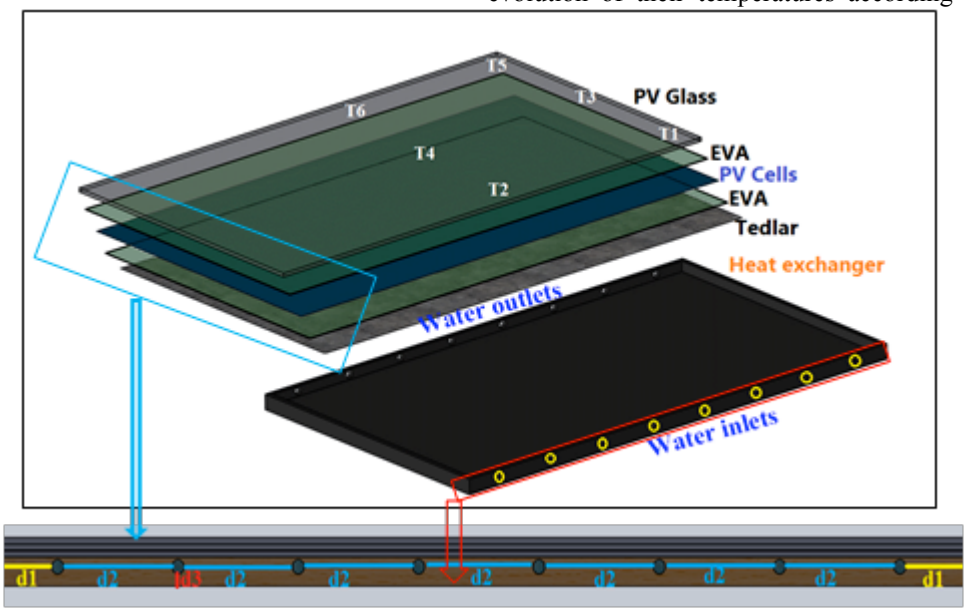

Fig. 4. PVT hybrid system with 8 (I/O). Opening diameter: d=6 mm; distance between openings: d2 = 68.75 mm; distance opening-Heat exchanger edge: d1 = 34.375mm; sheet water thickness: e= 8 mm.

conditions for the chosen configuration.

2.2.2. PV module modelling

Illuminated solar cell may be represented by an equivalent electrical circuit which, depending on the chosen model, includes a current generator, a number of diodes and ohmic resistors describing the processes of internal losses (R_{SH} and R_S). An external load resistor (R_C) is introduced to complete the equivalent circuit of the cell under operating conditions.

In this study, two solar cell models were considered, the simple single-diode model (MSE) [35], and the efficacious model [25]. Their equivalent circuits are schematized below (Fig.5), and (Fig.6):

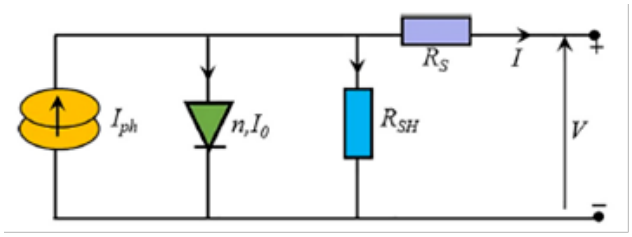

Fig. 5. PV module equivalent circuit corresponding to the MSE model

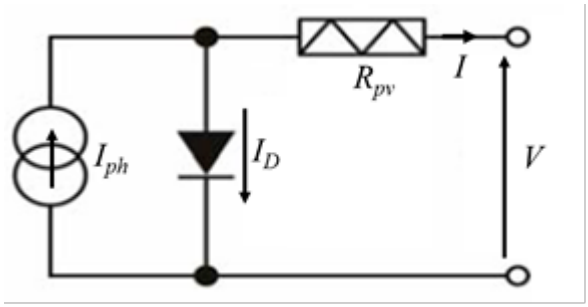

Fig. 6. PV module equivalent circuit corresponding to the efficacious model

The PV module current-voltage characteristic equation [36] in the case of MSE model is written as:

$$I = I_{ph} - I_0\left[\exp\left(\left(V + N_S R_S I\right)/\left(N_S n V_t\right)\right) - 1\right] - \left(V + N_S R_S I\right)/N_S R_{SH} \quad (5)$$

Where I_{ph}, I_0, n, and $V_t (= k_B T/q)$ are photogenerated current intensity, saturation current intensity, ideality factor, and thermal voltage, respectively. N_S is the number of cells connected in series, q is the charge of electron, and k_B is the Boltzmann constant.

Solar cell equivalent circuit corresponding to efficacious model (Fig. 6) is composed of a single diode and a fictitious resistor R_{PV} combining the two standard resistors (R_S , R_{SH}) [25]. Resolution of the current-voltage equation (Eq.6) required in this case the knowledge of only four parameters: R_{PV}, I_S, V_t and I_{ph}. Physical parameters n and R_{PV} can be determined by calculating the slope M (Eq.7), using experimental measurements of open circuit voltage (V_{OC}), short circuit current (I_{SC}) and those of current (I_m) and voltage (V_m) at maximum power point of the PV module.

$$I = I_{ph} - I_0\left(\exp\left(\left(V + IR_{pv}\right)/nV_t\right) - 1\right) \quad (6)$$

$$M = \left(dV/dI\right)\Big|_{I=0} = \left(V_{OC}/I_{SC}\right)\begin{pmatrix} -5.411\times\left(I_m \times V_m\right)/\left(I_{SC}\times V_{OC}\right) + \\ 6.450\times\left(V_m/V_{OC}\right) + 3.417\times\left(I_m/I_{SC}\right) \\ -4.422 \end{pmatrix} \quad (7)$$

$$n = -\left(\left(M + R_{PV}\right)I_{SC}/V_t\right) \quad (8)$$

$$R_{pv} = -M\left(I_{sc}/I_m\right) + \left(V_m/I_m\right)\left(1 - I_{SC}/I_m\right) \quad (9)$$

I_{ph} was evaluated as a function of solar irradiance (G) and T using the following equation [37–40]:

$$I_{ph} = \left(I_{ph,\mathrm{n}} + K_I\left(T - T_{\mathrm{n}}\right)\right)\left(G/G_{\mathrm{n}}\right) \quad (10)$$

$I_{ph,\mathrm{n}}$ is the photogenerated current intensity at STC: T_{n}=25 °C, G_{n}=1000 W/m^2. K_I is the short-circuit current temperature coefficient. Saturation current intensity I_0 depends on solar cell semiconductor material bandgap (E_g) and T [40–42], according to the following equation:

$$I_0(T) = I_{0,\mathrm{n}}\left(T/T_{\mathrm{n}}\right)^3 \exp\left[\left(qE_g/nk_B\right)\left(1/T_{\mathrm{n}} - 1/T\right)\right] \quad (11)$$

Where $I_{0,\mathrm{n}}$ is the intensity of nominal saturation current described by the following equation:

$$I_{0,\mathrm{n}} = \left(I_{SC,\mathrm{n}}/\exp\left(V_{OC,\mathrm{n}}/nV_{t,\mathrm{n}}\right) - 1\right) \quad (12)$$

$I_{SC,\mathrm{n}}$, $V_{OC,\mathrm{n}}$ and $V_{t,\mathrm{n}}$ are the STC physical parameters.

E_g was evaluated as a function of T using the following equation [43]:

$$E_g(T) = E_g(0) - \left(\alpha T^2/\left(T + \beta\right)\right) \quad (13)$$

Where $E_g(0)$, α and β are adjustment parameters.

The electrical efficiency is calculated using the following equation [44–49]:

$$\eta_{ele} = \eta_{ref}\left[1-\beta\left(T-25\right)\right] \quad (14)$$

Where: η_{ref}, and β are electrical efficiency at STC, and temperature correction coefficient (%/°C), respectively.

3. Results and discussion

Fig. 7 (a, b, c and d) show simulation results of the temperature stabilization process of the cooled PV module at 6 selected points (T1 to T6) for two configurations of the cooling system (4 I/O and 8 I/O) and two flow rates. With 8 I/O configuration and 0.8 L/min water flow (Fig. 7. (d)), a minimum temperature difference was reached throughout the surface of the cooled module. In this case the stabilization temperature was about 24 °C. The thermal image of the PV module surface (Fig. 9) seems to confirm this result.

Table 4 shows the simulated and measured temperature in the six points over the surface of the cooled module and those served as reference. Indeed, we can deduce from this table that there is about 3 °C of the difference between the measured temperatures and those simulated. This gap can be explained by the difference between the simulation conditions and the real outdoor operating conditions like the real thermal part in the solar spectrum which is converted in the heat by the PV module as well as the aleatory direction of the wind speed which affects the temperature stabilization on the PV module surface.

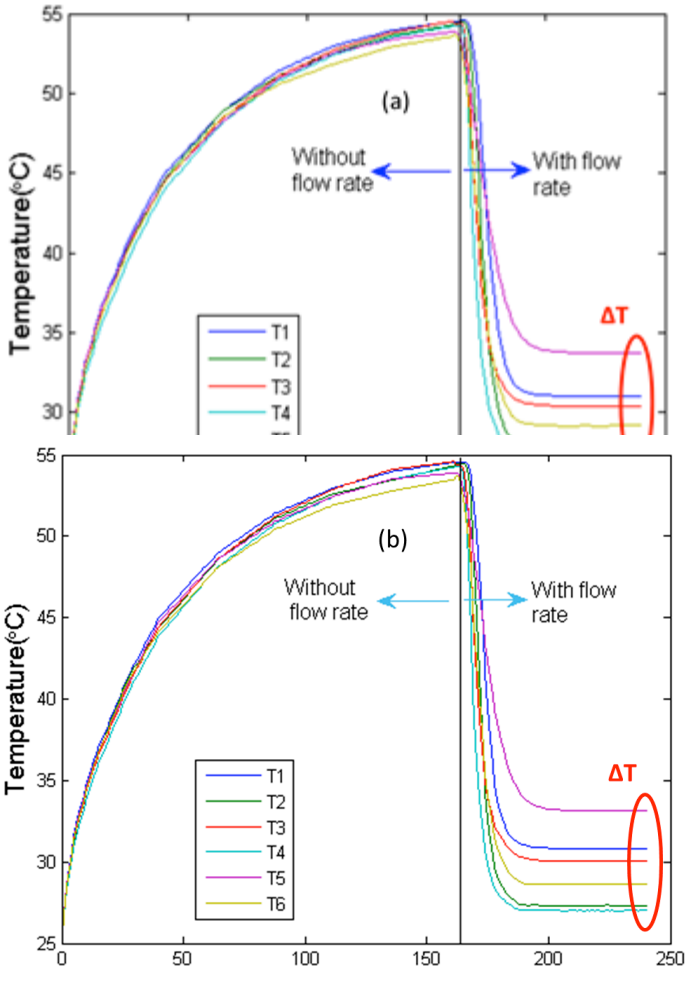

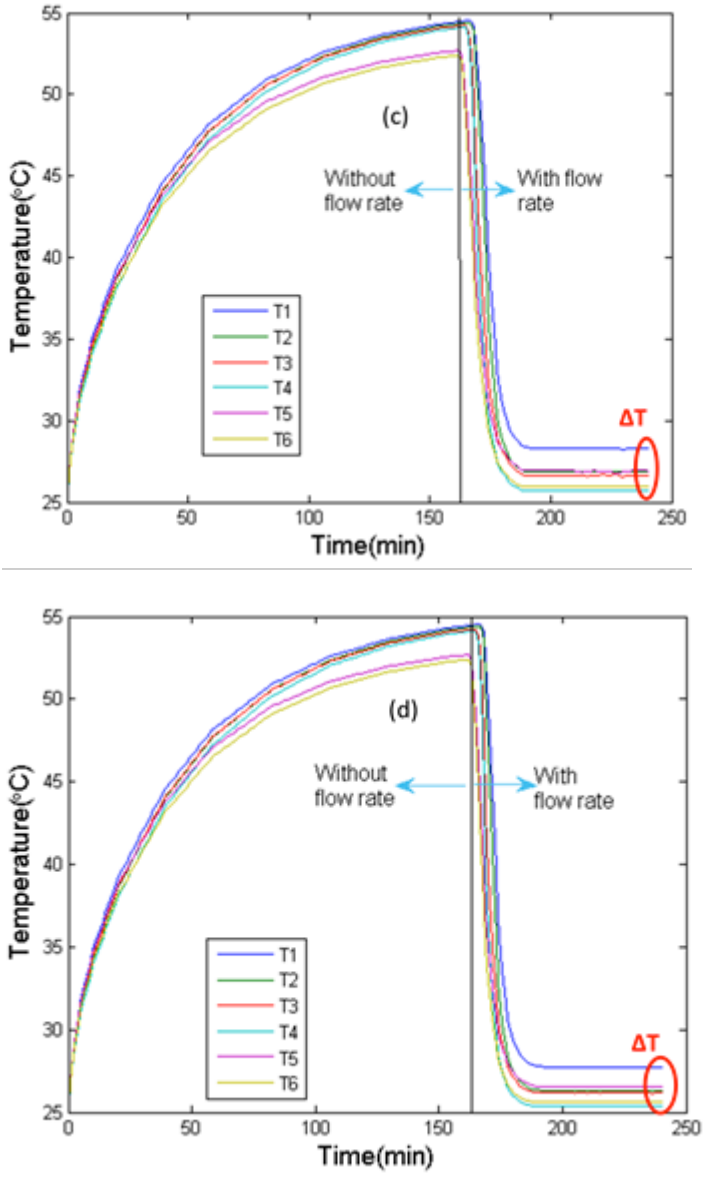

Fig. 7. Temperature evolution as a function of time at T1 to T6 points with flow rates of 0.6 L/min (a, c) and 0.8 L/min (b, d) for configurations, 4 (I/O) and 8 (I/O), respectively. Wind speed of 1.5 m/s, ambient temperature of 25 °C, solar irradiance of 830 W/m², inlet coolant temperature of 20 °C.

Electrical efficiency of the cooled PV module increased (Fig. 8) from 13.0 % to 14.1% when the PV module temperature decreased from 48 °C to 24 °C, which confirms the reliability of the cooling system. Using Eq. 14, the calculated temperature correction coefficient for the power was equal to -0.366 %/°C.

Table 5 shows the physical parameters (I_0, R_{pv}, n, and I_{ph}) evolution associated to the effective model as a function of temperature. R_{pv} can take positive or negative values and has no physical meaning. Operating point of the PV module can be determined with an accuracy of 2.7 %.

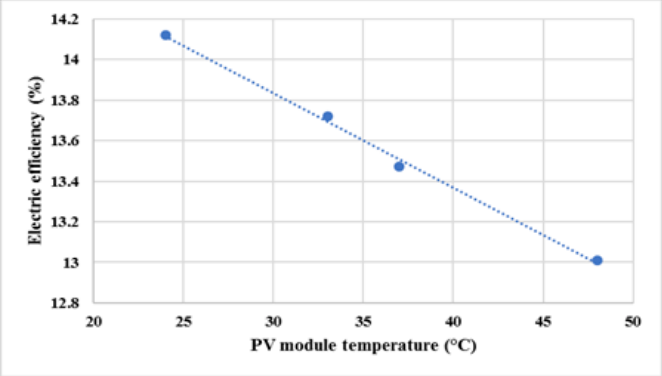

Fig. 8. Electrical efficiency as a function of the cooled module temperature

Table 4. Simulated and measured Temperature on the PV modules surface.

	Cooled Module			Reference Module
T(°C)	Simulated (a)	Measured (b)	Difference (a-b)	Measured
T_1	27.7	24.6	3.1	42.4
T_2	26.3	23.2	3.1	42.6
T_3	26.1	23	3.1	40
T_4	25.3	22.2	3.1	41.2
T_5	26.5	23.4	3.1	40
T_6	25.5	22.5	3	42

Table 5. Calculated physical parameters (I_0, R_{pv}, n, I_{ph}), with the efficacious model.

	PV module temperature (°C)	
	24	48
I_0 (A)	11.9×10^{-6}	33.3×10^{-6}
R_{pv} (Ω)	0.64	0.70
n	2.14	1.98
I_{ph} (A)	0.830	0.897

As can be seen from Fig. 9, the realized PVT system shows better temperature homogeneity on the PV module surface, which is very important for the PV module stability and lifetime.

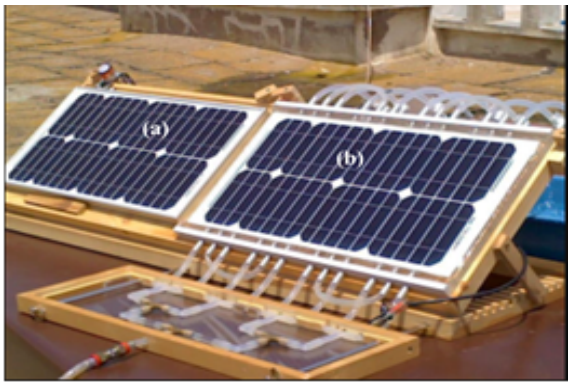

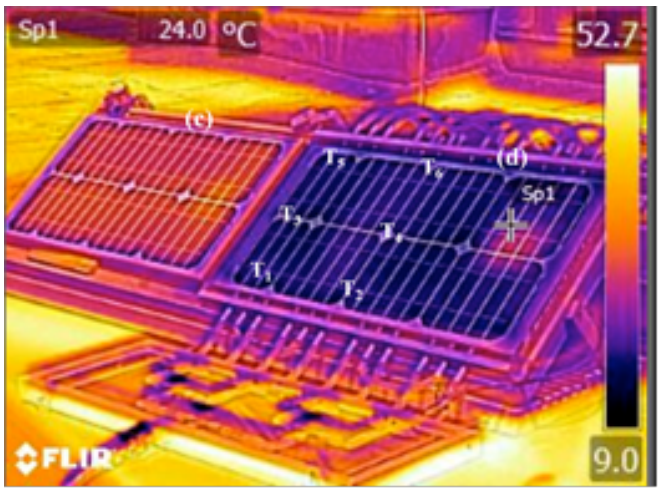

Fig. 9. Images of the reference module (a) and the cooled module (b). Thermal images of the reference PV module (c) and the cooled module (d).

The iterative injection method [50] consists of injecting test values of one (or more) physical parameter into (Eq.5) to generate a set of probable characteristics. Indeed, the ideality factor to be determined in the framework of the efficacious model was injected into the optimization program with the choice of an iteration interval around this value so that the optimization program converges rapidly. The parameter « $\%\Delta Area$ » defined by (Eq.15) below allows the evaluation of the relative difference between the experimental curve surface and those generated by:

$$\%\Delta Area = \left(\frac{\text{Surface of experimental characteristic curve - Surface of generated characteristic curve}}{\text{Surface of experimental characteristic curve}}\right)\times 100$$

The values of the extracted physical parameters by this method are those which correspond to the minimum value of $\%\Delta Area$ and which remains below 3% for intermediate temperatures (T = 33 °C and T = 37 °C). $\%\Delta Area$ closes to zero at the maximum power point (Fig. 10).

Fig. 11 shows physical parameters evolution of the cooled module with irradiance of 830 W/m^2 for temperatures of 24 °, 33 °, 37 ° and 48 °C. Module physical parameters were extracted using Ortiz-Condé method in the frame of the simple single-diode model. Increase in temperature causes increase of reverse saturation current I_0 and of charge carriers generation due to narrowing of bandgap (Eq.13), [51].

The decrease of n and R_{SH} values and the increase of that of R_S with increasing temperature (Fig. 12) are in good agreement with the literature results [41,42,52]. The variation of the ideality factor should depend on the PV module fabrication process, the localization, and density of traps levels in the semiconductor material [53].

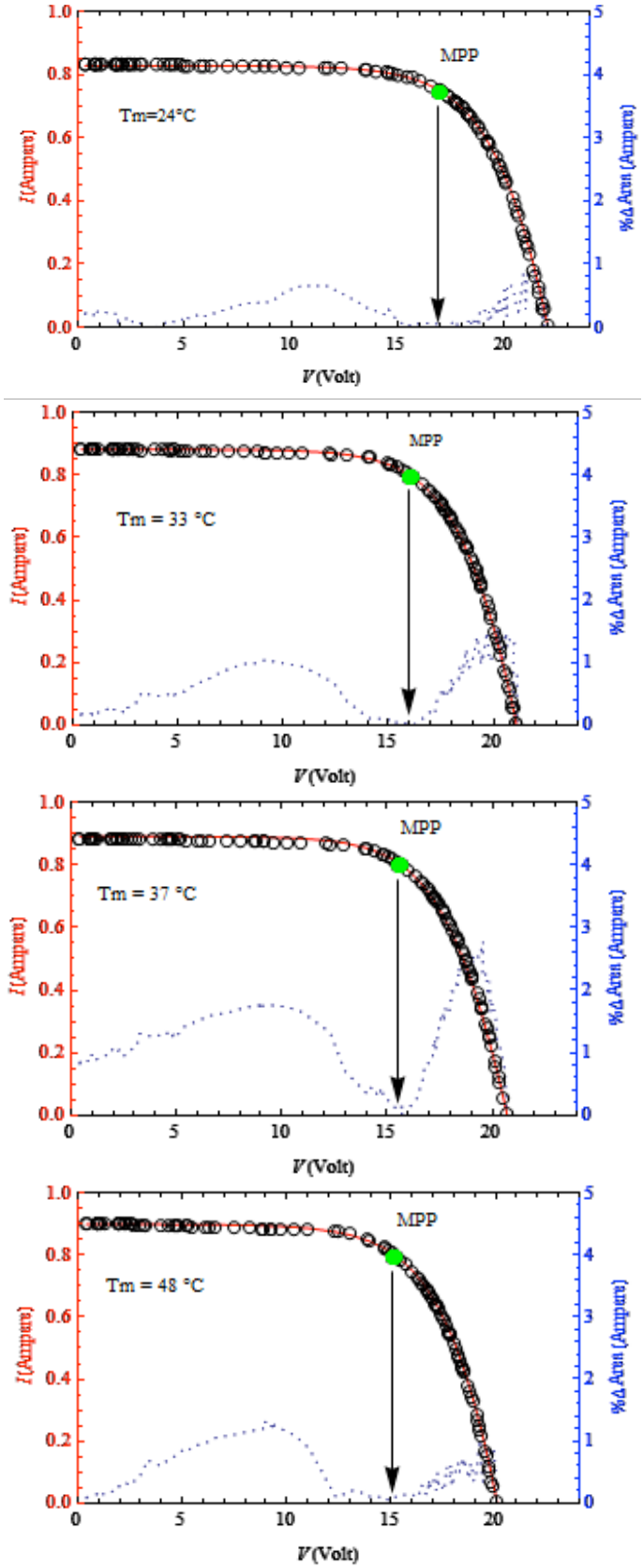

Fig. 10. *I-V* experimental characteristics (o), *I-V* characteristics plotted using physical parameters extracted within efficacious model (___) and $\%\Delta Area$ (.....).

Fig. 11 shows the experimental *I-V* characteristics of the cooled PV monocrystalline module for the four temperature values. As expected, the increase of the PV module temperature has a clear effect on V_{OC} and a slight increase of I_{SC}. Indeed, V_{OC} is proportional to the contact potential difference given by the following equation [54]:

$$V_D = \left(\frac{kT}{q}\right)\ln\left(\frac{N_D N_A}{n_i^2}\right) \tag{16}$$

Where $k, q, T, N_D, N_A,$ and n_i are Boltzmann's constant, electron charge, PV module temperature, donor atoms concentration, acceptor atoms concentration, and intrinsic carrier concentration, respectively. When the PV module temperature increases, the intrinsic concentration (n_i) increases rapidly, which consequently leads to the decrease of V_D and V_{OC}.

Otherwise, the short-circuit current is proportional to the number of generated charge carriers and their mobility. Furthermore, it highly depends on the generation rate and the diffusion length. Therefore, the increase of PV module temperature causes a slight increase of short circuit current [46]–[48]

.

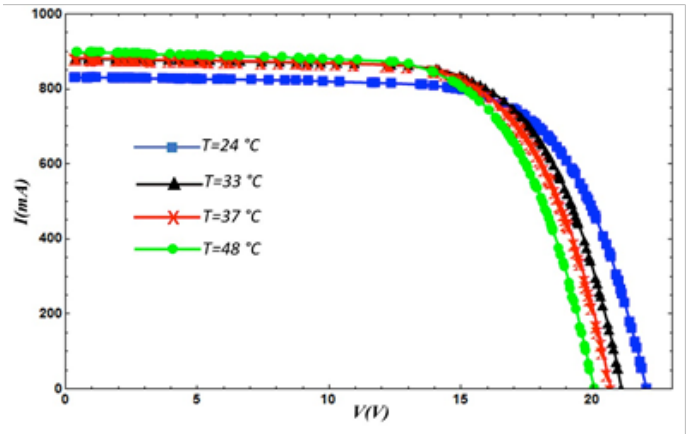

Fig. 11. Experimental I-V characteristics of the cooled PV module at different temperature values for G≈830 W/m².

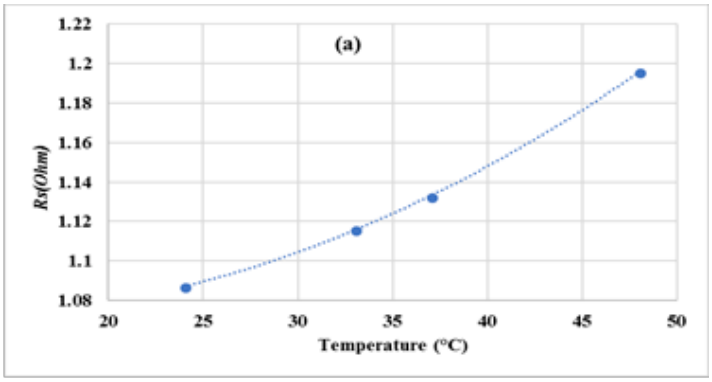

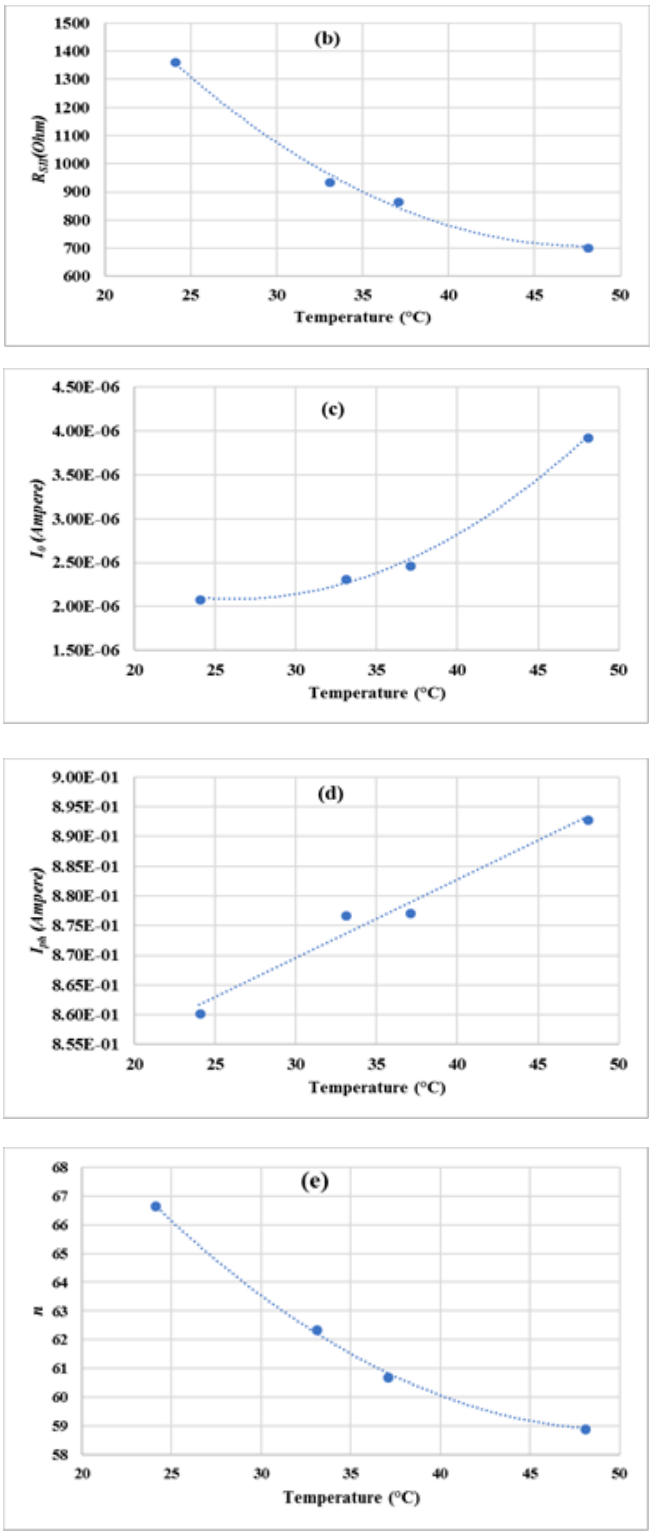

Fig. 12. Temperature influence on the PV module physical parameters. (a): R_S; (b): R_{SH}; (c): I_0; (d): I_{ph}; (e) :n.

I-V experimental characteristics, and those generated by extracted physical parameters using iterative and Ortiz-Condé (Fig. 13, (a) and (b)) methods exhibit good compatibility for operating temperatures of the module at 24°C, 33°C, 37°C and 48°C.

Fig. 14 ((a) and (b)) shows the current intensity error between the experimental characteristics and those obtained by the two used extraction methods.

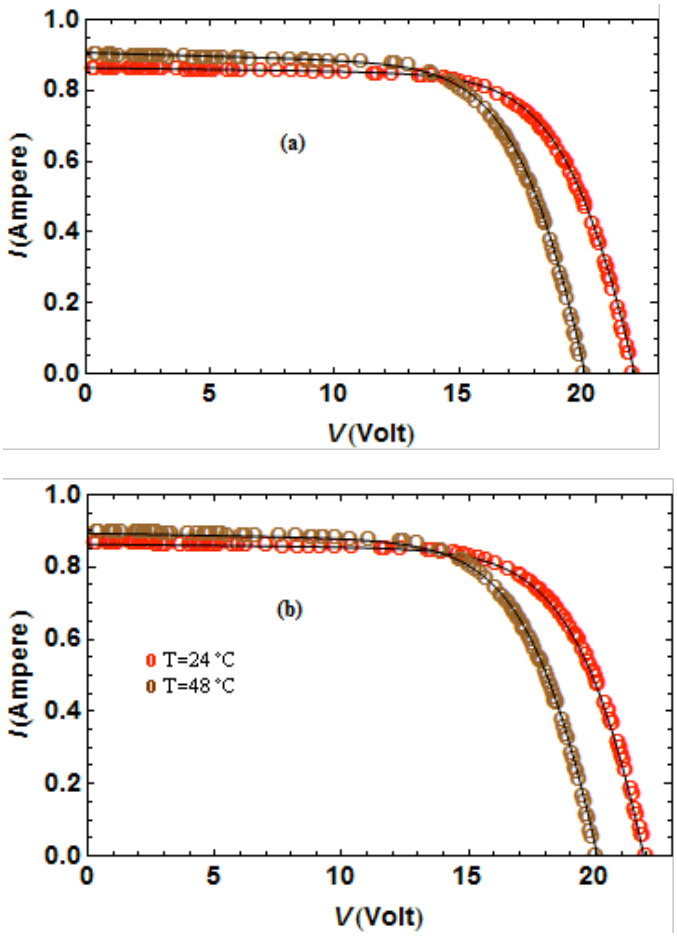

Fig. 13. (o) Experimental characteristics (I-V). Characteristics obtained by optimization (—) (MSE). (a): by iterative method; (b): by Ortiz-Condé method

As can be seen (Fig. 14), the iterative method gives a better agreement with the experimental measurements compared with Ortiz-Condé method.

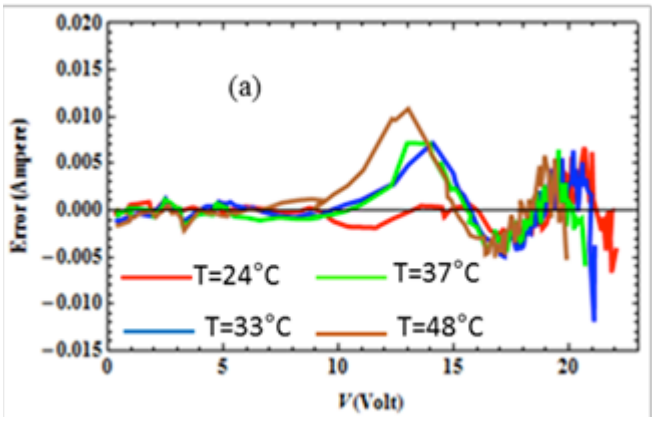

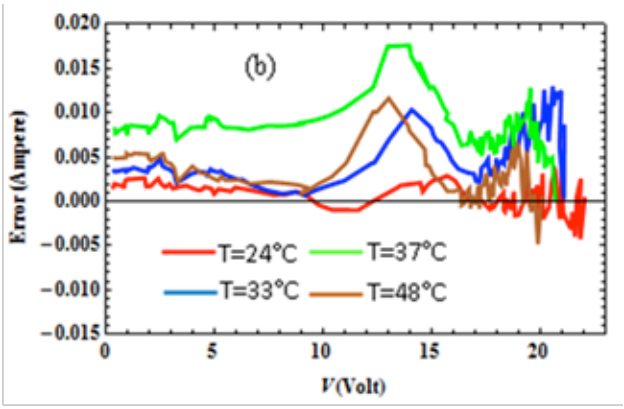

Fig. 14. Error between the experimental values of the current intensity and those deduced by (a) the iterative method and by (b) the Ortiz-Condé method.

4. Conclusion

This work involves the building of a PV module cooling system and the experimental validation of its optimal configuration determined by simulation based on finite element method.

The objective of the study was to control the temperature of the PV module and to minimize the temperature gradient along its receiving surface. The thermal image of the PV module receiving surface shows an evolution of temperature values fairly close to those obtained by simulation.

The built PVT cooling system allows to:

- decrease and control the PV module operating temperature of about 24 °C.
- limit the temperature difference along the PV module receiving surface to approximately 3 °C.
- improve the electrical efficiency by 0.046 %/°C when the PV module temperature decreases from 48 °C to 24 °C.
- check the behavior of the physical parameters (RS, RSH) as a function of the PV module temperature which result in an increase of RS with a rate of 4.6 mΩ/°C and a decrease of RSH with a rate of 27.5 Ω/°C. These results are in agreement with the expected effects of RS and RSH variations on the electrical efficiency.

It will be interesting to study the PVT system in an arid or semi-arid climate characterized by harsh climatic conditions and for other operating temperatures of the PV module.

Acknowledgements

The authors wish to express their gratitude to Prof. Yahya BENKHEDDA for proofreading the final version of the manuscript.

The authors express their gratefulness to CNRST (National Center for Scientific and Technical Research, Morocco) for the financial support provided to one of the authors of this study.

Reference:

[1] Skoplaki E, Palyvos JA. On the temperature dependence of photovoltaic module electrical performance: A review of efficiency/power correlations. Sol Energy 2009;83:614–24.

[2] Hazi A, Hazi G, Grigore R, Vernica S. Opportunity to use PVT systems for water heating in industry. Appl Therm Eng 2014;63:151–7.

[3] Ziapour BM, Palideh V, Mokhtari F. Performance improvement of the finned passive PVT system using reflectors like removable insulation covers. Appl Therm Eng 2016;94:341–9.

[4] Dupeyrat P, Ménézo C, Fortuin S. Study of the thermal and electrical performances of PVT solar hot water system. Energy Build 2014;68:751–5.

[5] Chow TT, He W, Ji J. An experimental study of façade-integrated photovoltaic/water-heating system. Appl Therm Eng 2007;27:37–45.

[6] Shi Q, Lv J, Guo C, Zheng B. Experimental and simulation analysis of a PV/T system under the pattern of natural circulation. Appl Therm Eng 2017;121:828–37.

[7] Hajjaj C, Amiry H, Bendaoud R, Yadir S, Elhassnaoui A, Sahnoun S, et al. Design of a new photovoltaic panel cooling system to optimize its electrical efficiency, IEEE; 2016, p. 623–627. doi:10.1109/IRSEC.2016.7983939.

[8] Sathe TM, Dhoble AS. A review on recent advancements in photovoltaic thermal techniques. Renew Sustain Energy Rev 2017;76:645–72. doi:10.1016/j.rser.2017.03.075.

[9] Preet S. Water and phase change material based photovoltaic thermal management systems: A review. Renew Sustain Energy Rev 2018;82:791–807. doi:10.1016/j.rser.2017.09.021.

[10] Alobaid M, Hughes B, Calautit JK, O'Connor D, Heyes A. A review of solar driven absorption cooling with photovoltaic thermal systems. Renew Sustain Energy Rev 2017;76:728–42. doi:10.1016/j.rser.2017.03.081.

[11] Al-Waeli AHA, Sopian K, Kazem HA, Chaichan MT. Photovoltaic/Thermal (PV/T) systems: Status and future prospects. Renew Sustain Energy Rev 2017;77:109–30. doi:10.1016/j.rser.2017.03.126.

[12] Brahim T, Jemni A. Economical assessment and applications of photovoltaic/thermal hybrid solar technology: A review. Sol Energy 2017;153:540–61. doi:10.1016/j.solener.2017.05.081.

[13] Elbreki AM, Alghoul MA, Sopian K, Hussein T. Towards adopting passive heat dissipation approaches for temperature regulation of PV module as a sustainable solution. Renew Sustain Energy Rev 2017;69:961–1017. doi:10.1016/j.rser.2016.09.054.

[14] Good C. Environmental impact assessments of hybrid photovoltaic–thermal (PV/T) systems – A review. Renew Sustain Energy Rev 2016;55:234–9. doi:10.1016/j.rser.2015.10.156.

[15] Lamnatou C, Chemisana D. Photovoltaic/thermal (PVT) systems: A review with emphasis on

environmental issues. Renew Energy 2017;105:270–87. doi:10.1016/j.renene.2016.12.009.

[16] Siecker J, Kusakana K, Numbi BP. A review of solar photovoltaic systems cooling technologies. Renew Sustain Energy Rev 2017;79:192–203. doi:10.1016/j.rser.2017.05.053.

[17] Simms S, Dorville J-F. Thermal performance of a hybrid photovoltaic-thermal collector with a modified absorber. 2015 Int. Conf. Renew. Energy Res. Appl. ICRERA, Palermo, Italy: IEEE; 2015, p. 600–5. doi:10.1109/ICRERA.2015.7418484.

[18] Tripanagnostopoulos Y, Nousia TH, Souliotis M, Yianoulis P. Hybrid photovoltaic/thermal solar systems. Sol Energy 2002;72:217–234.

[19] Chow TT, Pei G, Fong KF, Lin Z, Chan ALS, Ji J. Energy and exergy analysis of photovoltaic–thermal collector with and without glass cover. Appl Energy 2009;86:310–6.

[20] Yang DJ, Yuan ZF, Lee PH, Yin HM. Simulation and experimental validation of heat transfer in a novel hybrid solar panel. Int J Heat Mass Transf 2012;55:1076–82.

[21] Rossi C, Tagliafico LA, Scarpa F, Bianco V. Experimental and numerical results from hybrid retrofitted photovoltaic panels. Energy Convers Manag 2013;76:634–44.

[22] Michael JJ, S I, Goic R. Flat plate solar photovoltaic–thermal (PV/T) systems: A reference guide. Renew Sustain Energy Rev 2015;51:62–88.

[23] Liang R, Zhang J, Ma L, Li Y. Performance evaluation of new type hybrid photovoltaic/thermal solar collector by experimental study. Appl Therm Eng 2015;75:487–92.

[24] Fayaz H, Nasrin R, Rahim NA, Hasanuzzaman M. Energy and exergy analysis of the PVT system: Effect of nanofluid flow rate. Sol Energy 2018;169:217–30. doi:10.1016/j.solener.2018.05.004.

[25] Andreas W. Photovoltaik Engineering Handbuch für Planung, Entwicklung und Anwendung. Berlin Heidelberg New York: Springer-Verlag Berlin Heidelberg; 2006.

[26] Ortizconde A, Garciasanchez F, Muci J. New method to extract the model parameters of solar cells from the explicit analytic solutions of their illuminated characteristics. Sol Energy Mater Sol Cells 2006;90:352–61.

[27] Amiry H, Benhmida M, Bendaoud R, Hajjaj C, Bounouar S, Yadir S, et al. Design and implementation of a photovoltaic I-V curve tracer: Solar modules characterization under real operating conditions. Energy Convers Manag 2018;169:206–16. doi:10.1016/j.enconman.2018.05.046.

[28] Al-Hajj R, Assi A, Fouad MM. A predictive evaluation of global solar radiation using recurrent neural models and weather data. 2017 IEEE 6th Int. Conf. Renew. Energy Res. Appl. ICRERA, San Diego, CA: IEEE; 2017, p. 195–9. doi:10.1109/ICRERA.2017.8191265.

[29] Demirtas M, Yesilbudak M, Sagiroglu S, Colak I. Prediction of solar radiation using meteorological data. 2012 Int. Conf. Renew. Energy Res. Appl. ICRERA, Nagasaki, Japan: IEEE; 2012, p. 1–4. doi:10.1109/ICRERA.2012.6477329.

[30] Amiry H, Bendaoud R, Hajjaj C, Bounouar S, Yadir S, Rais K, et al. Temperature influence on performance of a solar cell receiving direct sunlight and a halogen lamp irradiation. IEEE Publ 2016:218–21.

[31] Armstrong S, Hurley WG. Response to comments by E. Sartori on "A thermal model for PV panels under varying atmospheric conditions", by S. Armstrong and WG Hurley, Applied Thermal Engineering 30, 1388–1395 (2010). Appl Therm Eng 2011;31:402.

[32] Chanaa F, Bendaoud R, Bounouar S, Hajjaj C, El-abidi A, Ezzaki H, et al. Design and Experimental Study of an Implemented Solar Air Heater Destined for Red Algae Drying. Int J Renew ENERGY Res 2018:2266–74.

[33] McAdams WH. Heat Transmission. New York: 1954.

[34] Naewngerndee R, Hattha E, Chumpolrat K, Sangkapes T, Phongsitong J, Jaikla S. Finite element method for computational fluid dynamics to design photovoltaic thermal (PV/T) system configuration. Sol Energy Mater Sol Cells 2011;95:390–3.

[35] Luque A, Hegedus S, editors. Handbook of photovoltaic science and engineering. 2nd ed. Chichester, West Sussex, U.K: Wiley; 2011.

[36] Abdelhakim B, Ilhami C, Korhan K. Modeling and simulation of thermo electrical generator with MPPT. 2017 IEEE 6th Int. Conf. Renew. Energy Res. Appl. ICRERA, San Diego, CA, USA: IEEE; 2018, p. 855–66. doi:10.1109/ICRERA.2017.8191181.

[37] Sera D, Teodorescu R, Rodriguez P. PV panel model based on datasheet values. IEEE Int. Symp. Ind. Electron., 2007, p. 2392–2396. doi:10.1109/ISIE.2007.4374981.

[38] Kajihara A, Harakawa T. Model of photovoltaic cell circuits under partial shading 2005.

[39] Benavides ND, Chapman PL. Modeling the effect of voltage ripple on the power output of photovoltaic modules. IEEE Trans Ind Electron 2008;55:2638–43.

[40] De Soto W, Sa K, Wa B. Improvement and validation of a model for photovoltaic array performance 2006.

[41] Arivuselvam L, Sakthi D, Sakthivel P, Anbarasan PM, Aroulmoji V. Irradiance Dependence on Performance of Dye Sensitized and V-Grooved Silicon Solar Cells. Int J Adv Sci Eng 2014;1:18–26.

[42] Wurefl P. Physics of Solar Cells: From Principles to New Concepts. 2005.

[43] Singh P, Ravindra NM. Temperature dependence of solar cell performance—an analysis. Sol Energy Mater Sol Cells 2012;101:36–45.

[44] de la Parra I, Muñoz M, Lorenzo E, García M, Marcos J, Martínez-Moreno F. PV performance modelling: A review in the light of quality assurance for large PV plants. Renew Sustain Energy Rev 2017;78:780–97. doi:10.1016/j.rser.2017.04.080.

[45] Hajjaj C, Alami Merrouni A, Bouaichi A, Benhmida M, Sahnoun S, Ghennioui A, et al. Evaluation, comparison and experimental validation of different PV power prediction models under semi-arid climate. Energy Convers Manag 2018;173:476–88. doi:10.1016/j.enconman.2018.07.094.

[46] Hajjaj C, Benhmida M, Sahnoun S, Merrouni AA, Ghennioui A, Benlarabi A, et al. A comparative study of PV modules performance between prediction models and experience in the Green Energy Park: crystalline technology n.d.:4.

[47] Hajjaj C, Zitouni H, Merrouni AA, Bouaichi A, Benhmida M, Ikken B, et al. Evaluation of Different PV Prediction Models. Comparison and Experimental Validation with One-Year Measurements at Ground Level. In: Tina GM, editor. Proc. 1st Int. Conf. Electron. Eng. Renew. Energy, vol. 519, Singapore: Springer Singapore; 2019, p. 617–22. doi:10.1007/978-981-13-1405-6_70.

[48] Charaf H. Experimental Validation of Non-Linear Empirical Model to Simulate the Photovoltaic Production Under Semi-Arid Climate. Case Study of Benguerir, Morocco. IEEE Publ 2018:1–5.

[49] Al-Shohani WAM, Al-Dadah R, Mahmoud S, Algareu A. Performance of a V-trough photovoltaic system. 2016 IEEE Int. Conf. Renew. Energy Res. Appl. ICRERA, Birmingham, United Kingdom: IEEE; 2016, p. 946–51. doi:10.1109/ICRERA.2016.7884474.

[50] Bendaoud R, Yadir S, Hajjaj C, Errami Y, Sahnoun S, Benhmida M, et al. Validation of a multi-exponential alternative model of solar cell and comparison to conventional double exponential model. IEEE Publ n.d.:319–22.

[51] Arjyadhara1 P, S.M2 A, Chitralekha3 JC. Analysis of Solar PV cell Performance with Changing Irradiance and Temperature. Int J Eng Comput Sci 2013:214–20.

[52] Singh P, Singh S, Lal M, Husain M. Temperature dependence of I–V characteristics and performance parameters of silicon solar cell. Sol Energy Mater Sol Cells 2008;92:1611–6.

[53] Stirn RJ. Junction characteristics of silicon solar cells, 1972, p. 72–82. doi:19730029409.

[54] Wen C, Fu C, Tang J, Liu D, Hu S, Xing Z. The influence of environment temperatures on single crystalline and polycrystalline silicon solar cell performance. Sci China Phys Mech Astron 2012;55:235–41. doi:10.1007/s11433-011-4619-z.

[55] Chander S, Purohit A, Sharma A, Nehra SP, Dhaka MS. Impact of temperature on performance of series and parallel connected mono-crystalline silicon solar cells. Energy Rep 2015;1:175–80. doi:10.1016/j.egyr.2015.09.001.

[56] Chander S, Purohit A, Sharma A, Arvind, Nehra SP, Dhaka MS. A study on photovoltaic parameters of mono-crystalline silicon solar cell with cell temperature. Energy Rep 2015;1:104–9. doi:10.1016/j.egyr.2015.03.004.